Cell Reports

Differential roles of CaMKII isoforms in phase separation with NMDA receptors and in synaptic plasticity

Graphical abstract

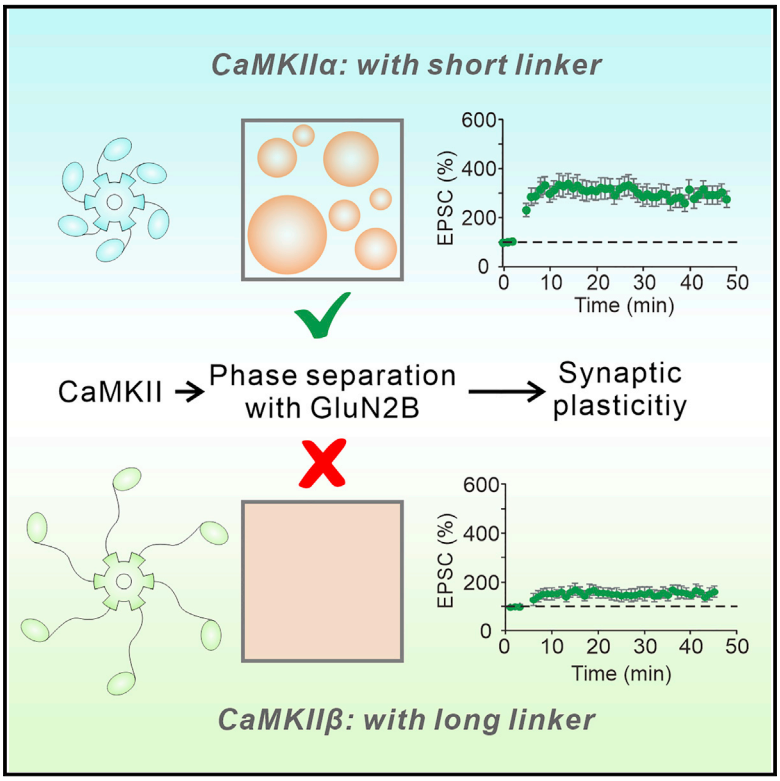

Highlights

- CaMKII with a short linker is critical to support basal synaptic transmission and LTP
- CaMKII with a short linker promotes phase separation with GluN2B
- The different roles of the CaMKII linker on phase separation are sequence independent

Authors

Qixu Cai, Xiumin Chen, Shihan Zhu, Roger A. Nicoll, Mingjie Zhang

Correspondence

roger.nicoll@ucsf.edu (R.A.N.), zhangmj@sustech.edu.cn (M.Z.)

In brief

CaMKIIα and CaMKIIβ play distinct roles in supporting synaptic transmission and LTP with unknown underlying mechanisms. Cai et al. show that the linker length of CaMKII determines its phase separation with GluN2B, which regulates its differential role in synaptic plasticity.

Cai et al., 2023, Cell Reports *42*, 112146
March 28, 2023
https://doi.org/10.1016/j.celrep.2023.112146

Cell Reports

CellPress
OPEN ACCESS

Report

Differential roles of CaMKII isoforms in phase separation with NMDA receptors and in synaptic plasticity

Qixu Cai,[1,2,5] Xiumin Chen,[3,5] Shihan Zhu,[1] Roger A. Nicoll,[3,*] and Mingjie Zhang[1,4,6,*]

[1]Division of Life Science, State Key Laboratory of Molecular Neuroscience, Hong Kong University of Science and Technology, Clear Water Bay, Kowloon, Hong Kong, China

[2]State Key Laboratory of Molecular Vaccinology and Molecular Diagnostics, Department of Laboratory Medicine, School of Public Heath, Xiamen University, Xiamen, Fujian 361102, China

[3]Department of Cellular and Molecular Pharmacology, University of California, San Francisco, San Francisco, CA 94143, USA

[4]School of Life Sciences, Southern University of Science and Technology, Shenzhen, Guangdong 518055, China

[5]These authors contributed equally

[6]Lead contact

*Correspondence: roger.nicoll@ucsf.edu (R.A.N.), zhangmj@sustech.edu.cn (M.Z.)

https://doi.org/10.1016/j.celrep.2023.112146

SUMMARY

Calcium calmodulin-dependent kinase II (CaMKII) is critical for synaptic transmission and plasticity. Two major isoforms of CaMKII, CaMKIIα and CaMKIIβ, play distinct roles in synaptic transmission and long-term potentiation (LTP) with unknown mechanisms. Here, we show that the length of the unstructured linker between the kinase domain and the oligomerizing hub determines the ability of CaMKII to rescue the basal synaptic transmission and LTP defects caused by removal of both CaMKIIα and CaMKIIβ (double knockout [DKO]). Remarkably, although CaMKIIβ binds to GluN2B with a comparable affinity as CaMKIIα does, only CaMKIIα with the short linker forms robust dense clusters with GluN2B via phase separation. Lengthening the linker of CaMKIIα with unstructured "Gly-Gly-Ser" repeats impairs its phase separation with GluN2B, and the mutant enzyme cannot rescue the basal synaptic transmission and LTP defects of DKO mice. Our results suggest that the phase separation capacity of CaMKII with GluN2B is critical for its cellular functions in the brain.

INTRODUCTION

Calcium calmodulin-dependent kinase II (CaMKII) and long-term potentiation (LTP) were discovered within a decade of each other and have been linked together ever since.[1–4] On the one hand, CaMKII provides a molecular basis for information storage in that a brief pulse of Ca^{2+} results in the long-lasting activation of the kinase. On the other hand, LTP, in which a brief high-frequency synaptic stimulation results in the long-lasting potentiation of synaptic responses, provides an attractive physiological readout for the underlying molecular changes. Indeed, it is well established that CaMKII activation is required for LTP,[5–9] and recent evidence indicates that it is required for the maintenance of LTP.[10–12]

However, there are two isoforms of neuronal CaMKII, CaMKIIα and CaMKIIβ, and they are expressed in the forebrain in a ratio of approximately 3:1.[13–15] CaMKII is extremely abundant in brains. At excitatory synapses of mature rodent brains, CaMKII is ~10 times more abundant than PSD-95.[16] Furthermore, holoenzymes are composed of both isoforms.[13–15] Both CaMKIIα and CaMKIIβ have an N-terminal kinase domain followed by an autoinhibitory sequence (AIS), followed by a linker domain that links the kinase domain with the C-terminal hub or association domain (Figure 1A). The hub domain assembles the individual subunits into a primarily dodecameric holoenzyme with a small population of tetradecamers or even higher oligomers.[17–20] Much of our understanding of CaMKII comes from studies on the α isoform. Genetic deletion of CaMKIIα severely impairs LTP,[7–9,21,22] and constitutively active CaMKIIα mimics LTP.[23,24] While genetic deletion of CaMKIIβ reduces LTP,[7,25,26] it is incapable of rescuing the defects seen when both isoforms are deleted together.[7] What could account for these profound differences? The structures and biochemical properties of CaMKIIα and CaMKIIβ are remarkably similar, in line with the extremely high amino acid sequence identity between the kinase and the hub domains of the isoforms.[1,2] In addition, both CaMKIIα[27–30] and CaMKIIβ (Bayer et al.[31] and this study below) bind to the C-terminal domain of the GluN2B subunit of the NMDA receptor (NMDAR). Direct binding between CaMKIIα and GluN2B is critical for basal AMPAR transmission[7,11] and LTP.[7,11,32,33] The primary difference between CaMKIIα and CaMKIIβ resides in the linker region. In the mouse brain and in the human hippocampus, the principle α isoform contains 30 amino acids and the β isoform contains 93 amino acids in their linkers.[18,34] The length of the

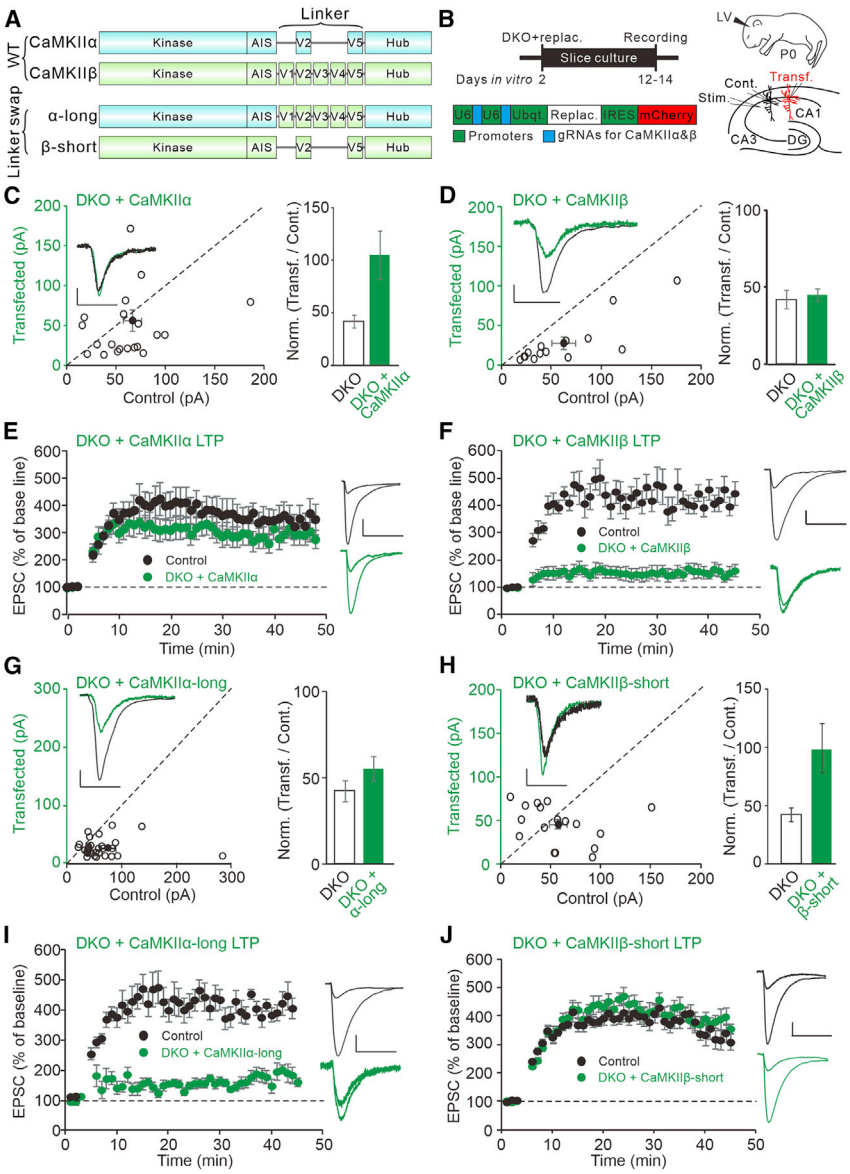

Figure 1. CaMKII with a short linker can rescue the defects of basal synaptic transmission and LTP induced by deletion of both CaMKIIα and CaMKIIβ (DKO)

(A) Schematic diagram showing the domain organization of CaMKIIα, CaMKIIβ, and various chimeric constructs of CaMKII.

(B) Timelines of experiments and schematic diagrams showing the electrophysiological approaches. Control represents the wild-type, untransfected neurons.

(C) Scatterplot and bar graph of ratios normalized to control of the AMPAR excitatory postsynaptic currents (EPSCs) for single pairs (open circles) of control and transfected cells of DKO + CaMKIIα. Filled circles indicate mean amplitude ± SEM (control = 66.1 ± 9.4; DKO + CaMKIIα = 57.1 ± 13.2, n = 21, p = 0.79). Bar graph of ratios normalized the control (%) summarizing the mean ± SEM of AMPAR EPSCs (104.6 ± 24).

(D) Scatterplot and bar graph of ratios normalized to control of the AMPAR EPSCs for single pairs (open circles) of control and transfected cells of DKO + CaMKIIβ. Filled circles indicate mean amplitude ± SEM (control = 61.7 ± 11.9; DKO + CaMKIIβ = 28.1 ± 7.1, n = 16, p < 0.001). Bar graph of ratios normalized to the control (%) summarizing the mean ± SEM of AMPAR EPSCs (45.5 ± 4).

(E and F) Plots show mean ± SEM AMPAR EPSC amplitude of control (black) and transfected (green) DKO + CaMKIIα (E) or DKO + CaMKIIβ (F) pyramidal neurons normalized to the mean AMPAR EPSC amplitude before LTP induction (E, control, n = 8; DKO + CaMKIIα, n = 8; F, control, n = 9; DKO + CaMKIIβ, n = 8).

(G) Scatterplot and bar graph of ratios normalized to control of the AMPAR EPSCs for single pairs (open circles) of control and transfected cells of DKO + CaMKIIα-long. Filled circles indicate mean amplitude ± SEM (control = 74.2 ± 14.5; DKO + CaMKIIα-long = 26.9 ± 2.7, n = 31, p < 0.001). Bar graph of ratios normalized to the control (%) summarizing the mean ± SEM of AMPAR EPSCs (55.4 ± 7).

(H) Scatterplot and bar graph of ratios normalized to control of the AMPAR EPSCs for single pairs (open circles) of control and transfected cells of DKO + CaMKIIβ-short. Filled circles indicate mean amplitude ± SEM (control = 50.1 ± 8.4; DKO + CaMKIIβ-short = 44.6 ± 5.3, n = 16, p = 0.85). Bar graph of ratios normalized to the control (%) summarizing the mean ± SEM of AMPAR EPSCs (109.2 ± 21).

(I and J) Plots show mean ± SEM AMPAR EPSC amplitude of control (black) and transfected (green) DKO + CaMKIIα-long (I) or DKO + CaMKIIβ-short (J) pyramidal neurons normalized to the mean AMPAR EPSC amplitude before LTP induction (I, control, n = 8; DKO + CaMKIIα-long, n = 8; J, control, n = 8; DKO + CaMKIIβ-short, n = 8). Raw amplitude data from dual-cell recordings were analyzed using Wilcoxon signed rank test (p values above). Scale bars: 20 ms, 50 mA.

linker in CaMKII has been linked to rates of autophosphorylation and dephosphorylation of T286 and T305/T306 of the enzyme.[35]

To determine if the linker region can account for the profound differences in the function of CaMKIIα and CaMKIIβ, we attempted to rescue the defects created by deleting both CaMKIIα and CaMKIIβ (double knockout [DKO])[7] by expressing mutant forms of the isoforms with variable linker lengths. We found that the ability of CaMKII mutants to rescue basal synaptic transmission, as well as LTP, was entirely related to the length of the linker. We further found a dramatic difference in the ability of CaMKIIα and CaMKIIβ to undergo phase separation with GluN2B, although both isoforms bind to GluN2B with comparable affinities. We postulate that the binding of CaMKII to GluN2B is not sufficient for its synaptic action. CaMKII's action also requires phase separation to form densely clustered protein condensates with NMDARs.

RESULTS

CaMKII with a short linker is critical to support basal synaptic transmission and LTP

Previous studies have shown that CaMKIIα and CaMKIIβ (Figure 1A) play different roles in basal synaptic transmission and LTP.[7] Using a previously well-established system in which both

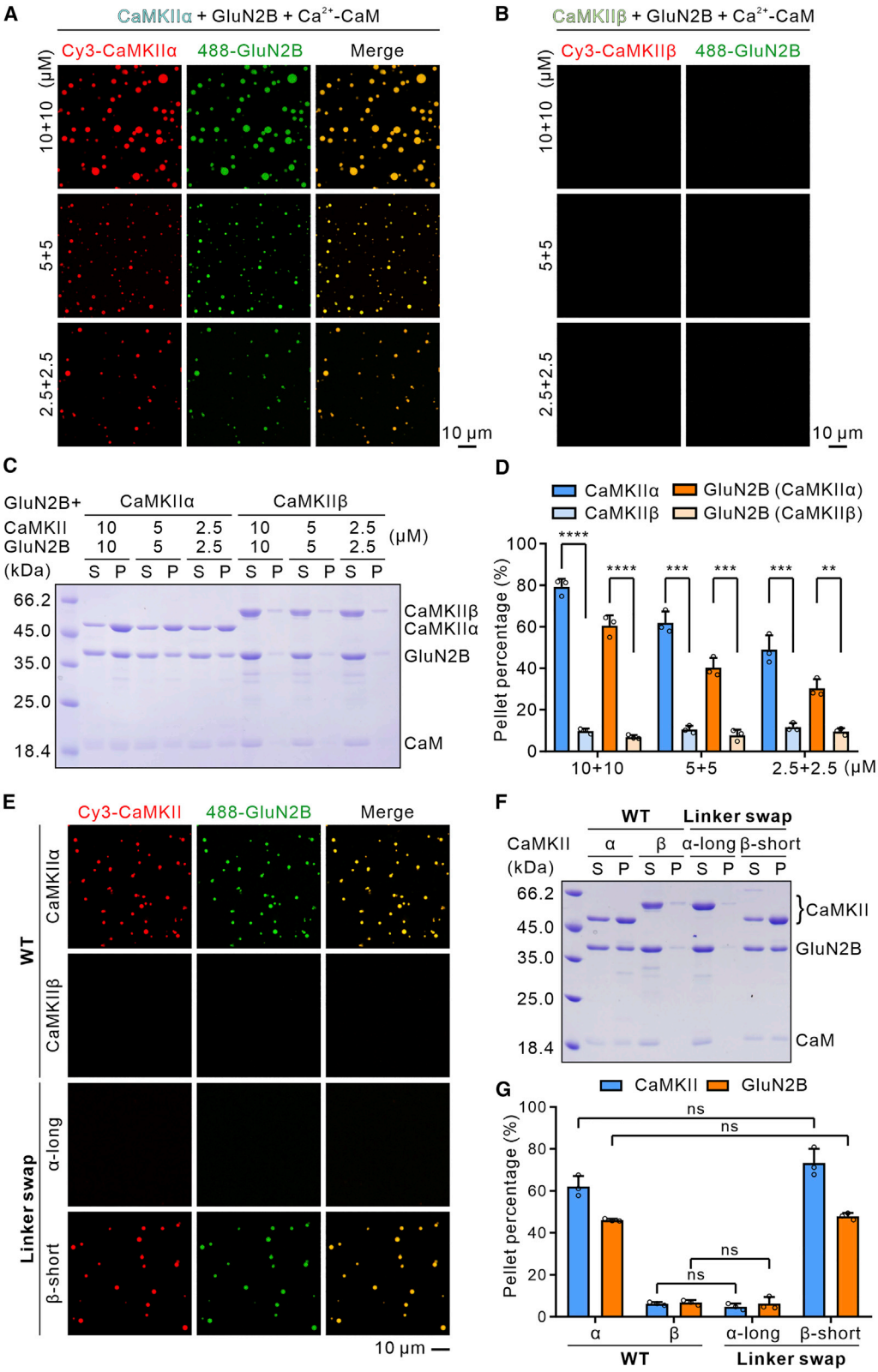

(legend on next page)

CaMKIIα and CaMKIIβ are deleted via CRISPR by two specific guide RNAs (gRNAs)[7] (Figure 1B), CaMKIIα fully rescued both basal transmission (Figure 1C) and LTP (Figure 1E) in the CA1 hippocampus neurons, whereas CaMKIIβ could not (Figures 1D and 1F).

The long linker of CaMKIIβ is encoded by five exons (V1–V5), and the short linker of CaMKIIα only contains exon V2 and V5 (Figure 1A).[36] To determine whether the different roles of CaMKIIα and CaMKIIβ in basal synaptic transmission and LTP are due to the different linker length, we generated two linker-swapped mutants of CaMKII, "CaMKIIα-long" (i.e., with the long linker from CaMKIIβ) and "CaMKIIβ-short" (i.e., with the V1, V3, and V4 exons deleted to make the length of linker the same as that of CaMKIIα) (Figure 1A). While CaMKIIα-long failed to rescue either basal synaptic transmission (Figure 1G) or LTP (Figure 1I), CaMKIIβ-short fully rescued both basal synaptic transmission (Figure 1H) and LTP (Figure 1J), indicating that the switch of the linkers between CaMKIIα and CaMKIIβ can fully account for the profound functional differences in these two isoforms.

CaMKII with a short linker promotes phase separation with GluN2B

Next, we sought to explain why CaMKIIα and CaMKIIβ have such a profound functional difference in supporting basal synaptic transmission and LTP. Previous research has established that the binding of CaMKIIα to GluN2B, one of the subunits of the NMDAR, is critical for the function of CaMKII.[7,32,33] The quantitative isothermal titration calorimetry (ITC) data revealed that the interactions between CaMKIIα and GluN2B or between CaMKIIβ and GluN2B were nearly the same (Figures S1A–S1D). We also used a purified GST-tagged GluN2B C-terminal domain (CTD) fragment containing aa 1259–1310 (termed GST-GluN2B in the figure) (Figure S1E) to pull down GFP-tagged CaMKIIα, CaMKIIβ, CaMKIIα-long, and CaMKIIβ-short expressed in heterologous cells, and the result showed that all four variants bound to GluN2B with a similar affinity (Figure S1E), indicating that the linker length does not influence the binding between CaMKII and GluN2B. In striking contrast, CaMKIIβ and CaMKIIβ-short failed to bind to the Shank3 NTD-ANK tandem (Figure S1E), as the kinase domain and a short fragment immediately following the kinase domain of CaMKIIα are responsible for the specific binding between CaMKIIα and Shank3.[37]

Previously, we reported that the CaMKIIα and GluN2B mixture can undergo phase separation,[37,38] prompting the question as to whether CaMKIIβ and GluN2B may also undergo phase separation. We sparsely labeled CaMKII variants and GluN2B CTD containing aa 1170–1482 (termed GluN2B) with Cy3-NHS and iFluor488-NHS, respectively. When mixed at room temperature, both CaMKIIα and GluN2B were highly enriched in the condensed droplets formed via phase separation in confocal fluorescence imaging experiments (Figure 2A). Remarkably, no condensed droplets could be observed in the mixture of CaMKIIβ and GluN2B (Figure 2B). This result indicated that, in sharp contrast to CaMKIIα, CaMKIIβ could not phase separate with GluN2B. The sedimentation-based experiments also showed the same result that CaMKIIα, but not CaMKIIβ, could phase separate with GluN2B (Figures 2C and 2D).

We then assayed the linker-swapped variants of CaMKII, CaMKIIα-long and CaMKIIβ-short, to test whether phase separation of CaMKII and GluN2B depend on the lengths of their linkers. Both confocal fluorescence imaging and sedimentation-based assays showed that the CaMKIIα-long mutant could not form droplets upon mixing with GluN2B. In contrast, the CaMKIIβ-short variant gained phase separation capacity upon binding to GluN2B (Figures 2E–2G). The results from the phase separation experiments shown in Figure 2 correlate very well with the functional results in Figure 1 showing that CaMKII with a short linker is critical for basal synaptic transmission and LTP.

CaMKIIα is stronger than CaMKIIβ in promoting phase separation of GluN2B with reconstituted 4×PSD

Formation of postsynaptic density (PSD) assemblies are driven by specific multivalent interactions between major PSD scaffold proteins via phase separation.[39,40] Hence, we asked whether CaMKIIα can still show stronger phase separation than CaMKIIβ when the other major PSD scaffold proteins (i.e., PSD-95, SAPAP, Shank3, and Homer3, termed 4×PSD; Figure S2A)[40] are incorporated into the phase separation system. Confocal fluorescence imaging studies indicated that although both CaMKIIα/GluN2B and CaMKIIβ/GluN2B could be recruited into reconstituted 4×PSD condensed droplets (Figure S2B), CaMKIIα promoted much stronger phase separation of both CaMKIIα and the other PSD proteins (Figure S2C). A sedimentation-based assay also supported the same conclusion (Figures S2D and S2E). Therefore, in a more complete reconstituted PSD system, CaMKIIα has a stronger phase separation capacity than CaMKIIβ.

Figure 2. CaMKII with a short linker promotes phase separation with GluN2B

(A and B) Confocal fluorescence images showing that CaMKIIα (A), but not CaMKIIβ (B), underwent phase separation with GluN2B in the present of Ca^{2+}-CaM at the indicated concentrations. The NaCl concentration included in the assay buffer was 100 mM. Only 1% of each protein was labeled by the indicated fluorophores. The NaCl concentration in the assay buffer and the fluorophore labeling ratio were kept the same throughout this study.

(C and D) Representative SDS-PAGE analysis (C) and quantification data (D) showing the distributions of CaMKII and GluN2B in the supernatant (S) and pellet (P) in the sedimentation-based assays with the indicated protein concentrations. The S and P fractions represent proteins in the dilute and condensed phases, respectively.

(E) Confocal fluorescence images showing that CaMKIIβ-short had an enhanced phase separation with GluN2B, whereas CaMKIIα-long showed a weakened phase separation with GluN2B. The final concentration of each protein in the assay was at 5 μM.

(F and G) Representative SDS-PAGE analysis (F) and quantification data (G) showing the distributions of CaMKII and GluN2B in the S and P in the sedimentation-based assay. The concentration of each protein in the assay was at 5 μM.

Statistical data in (D) and (G) are presented as mean ± SD, with results from 3 independent batches of sedimentation experiments. ns, not significant; $^{**}p < 0.01$; $^{***}p < 0.001$; $^{****}p < 0.0001$ using two-tailed Student's t test (D) and one-way ANOVA with Tukey's multiple comparisons test (G).

See also Figures S1 and S2.

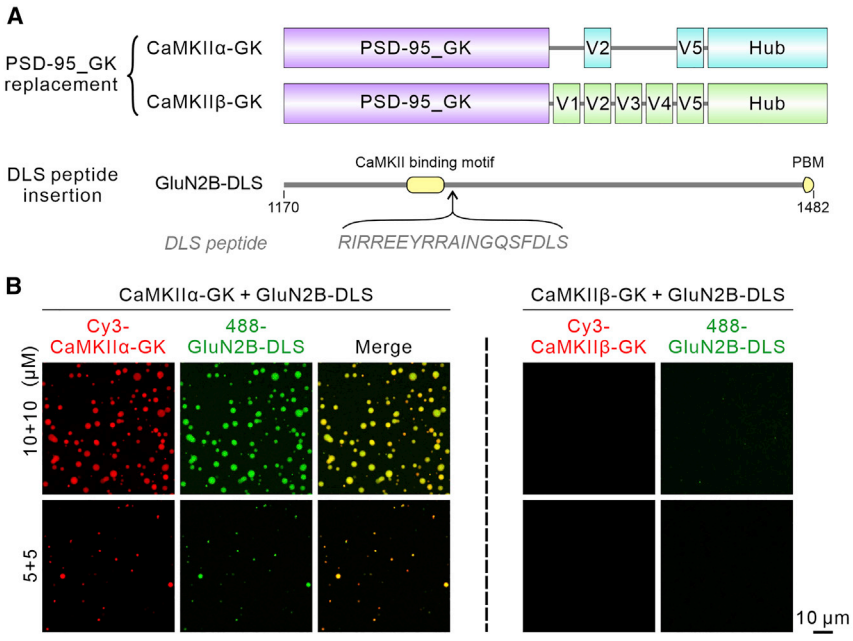

Figure 3. Phase separation of chimeric CaMKII-GK and GluN2B-DLS showing the critical role of the short linker in CaMKII for its phase separation with GluN2B

(A) Schematic diagram showing the domain organization of CaMKII with its kinase domain and AIS domain replaced by the GK domain of PSD-95 and GluN2B with the DLS peptide inserted after the CaMKII binding motif.

(B) Confocal fluorescence images showing that CaMKIIα-GK, but not CaMKIIβ-GK, underwent phase separation with GluN2B_DLS at the indicated concentrations.

(C and D) Representative SDS-PAGE analysis (C) and quantification data (D) showing the distributions of CaMKII-GK and GluN2B-DLS in the S and P in the sedimentation-based assays with the indicated protein concentrations.

Statistical data in (D) are presented as mean ± SD, with results from 3 independent batches of sedimentation experiments. ***$p < 0.001$; ****$p < 0.0001$ using two-tailed Student's t test.

See also Figure S3.

Phase separation of chimeric CaMKII-GK and GluN2B-DLS shows the critical role of the short linker of CaMKII for phase separation

Might the enhancement of phase separation by the short linker require the kinase domain coupling to the hub domain or kinase domain-kinase domain interactions?[18,19] To answer this question, we generated a CaMKII chimera with its kinase domain and AIS domain replaced by the GK domain of PSD-95, which we refer to as "CaMKII-GK" (Figure 3A). In parallel, a GluN2B chimera with a high-affinity short GK-binding peptide (called the DLS peptide as reported in our earlier study[41]) inserted after the CaMKII binding motif of GluN2B was also created, and the chimera is termed as "GluN2B-DLS" (Figure 3A). The binding between the PSD-95 GK domain from the CaMKII-GK chimera and the DLS peptide from the GluN2B-DLS chimera can functionally replace the binding between the kinase domain of CAMKII and CaMKII-binding motif of GluN2B in the native proteins.

Using these chimeric proteins, we could test whether the interactions between the kinase domains or between the kinase domain and the hub domain of CaMKII might also be required for the phase separation between CaMKII and GluN2B. Both imaging- (Figure 3B) and sedimentation-based experiments (Figures 3C and 3D) demonstrated that CaMKIIα-GK could undergo phase separation with GluN2B-DLS without Ca^{2+}-CaM, whereas CaMKIIβ-GK could not. On the other hand, the control experiments showed that both GK and DLS are necessary for the phase separation of chimeric CaMKII-GK and GluN2B-DLS, as no phase separation occurred when we mixed CaMKIIα with GluN2B-DLS or CaMKIIα-GK with GluN2B without Ca^{2+}-CaM (Figure S3). Thus, the short linker in CaMKII determines its phase separation with GluN2B, and the binding between the kinase domain and GluN2B is required and sufficient for the CaMKII/GluN2B complex to undergo phase separation.

The different roles of the CaMKII linker on phase separation is sequence independent

There are two possible interpretations of the results on the basal synaptic transmission and LTP rescue experiments in Figure 1 and the phase separation experiments above. First, the linker regions in CaMKIIβ, which are not present in CaMKIIα, might exert a specific negative role on CaMKII function. Alternatively, the inability of CaMKIIβ to rescue function may simply be due to the length of the linker. One of the differences between CaMKIIα and CaMKIIβ is that CaMKIIβ can specifically bind to F-actin, a property determined largely by the specific sequence of the V1 exon of CaMKIIβ.[25,26,36,42,43] Thus, we asked whether the different capacities of CaMKIIα and CaMKIIβ in phase separating with GluN2B might also be controlled by the specific sequences in their linkers and whether the F-actin binding ability of CaMKIIβ negatively regulate the rescue of basal synaptic transmission and LTP. We designed an artificial CaMKII construct termed CaMKIIα-GGS by inserting two fragments of "GlyGlySer" repeats with the same lengths of the V1 and V3–V4 exons of CaMKIIβ, respectively, into the CaMKIIα linker region (Figure 4A). The resulting CaMKIIα-GGS is with a linker of

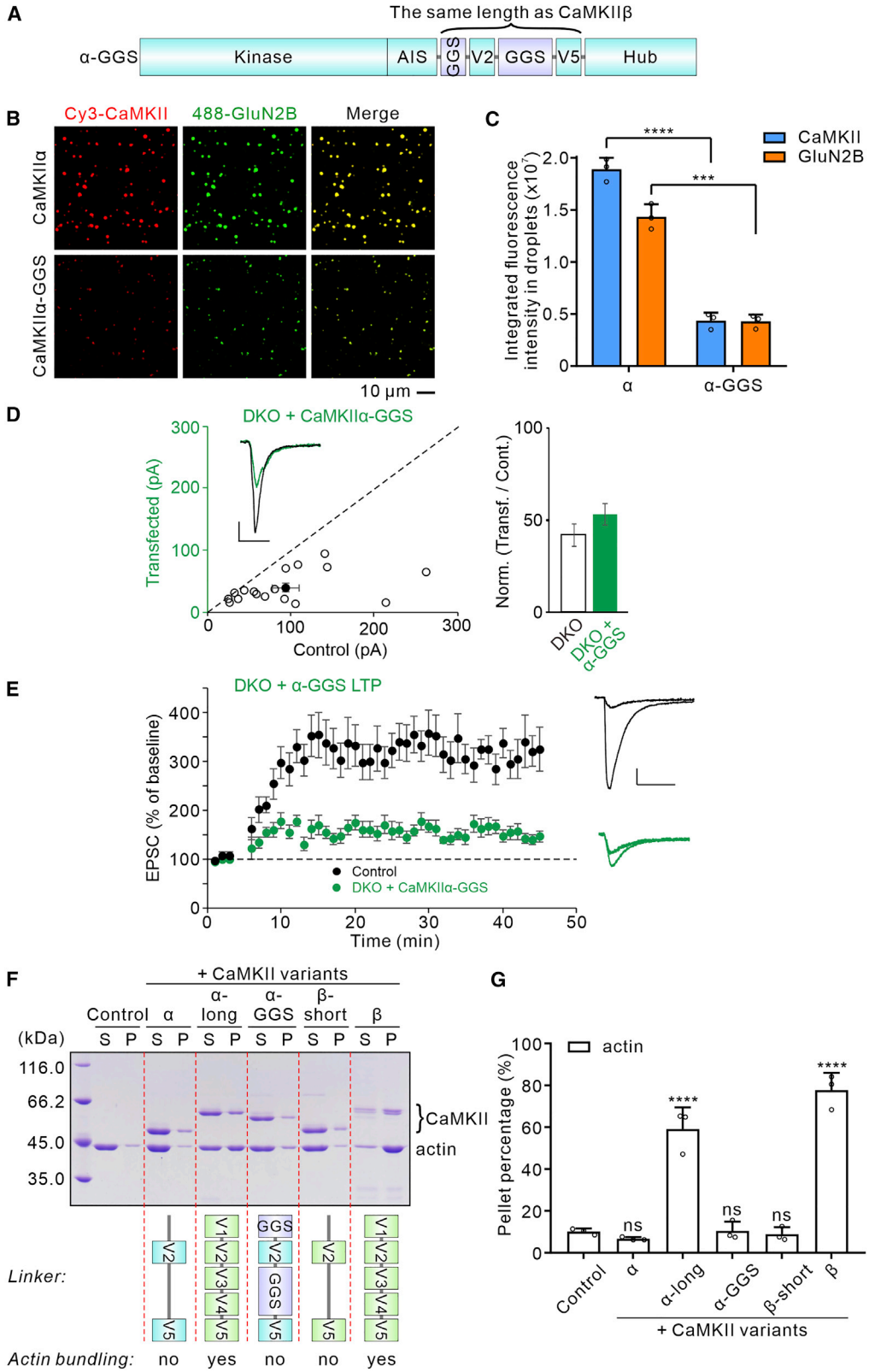

(legend on next page)

the same length to that of CaMKIIβ but without F-actin binding capacity (see below).

The imaging-based phase separation assay revealed that, compared with CaMKIIα, CaMKIIα-GGS has a much lower capacity in forming condensed droplets with GluN2B (Figures 4B and 4C), consistent with our theory that it is the linker length that determines the phase separation of CaMKII with GluN2B. We also demonstrated that CaMKIIα-GGS, like other CaMKII variants with the long linker (i.e. CaMKIIα-long and CaMKIIβ), failed to rescue basal synaptic transmission (Figure 4D) and LTP (Figure 4E) in the DKO neurons. Thus, the roles of the long linker of CaMKII variants in both phase separation and electrophysiological functions are amino acid-sequence independent.

It is possible that the reason CaMKIIβ and CaMKIIα-long cannot rescue basal transmission and LTP in CaMKII DKO neurons is due to both of them bundling F-actin instead of their weak phase separation with GluN2B. To address this question, we performed sedimentation-based F-actin bundling assays to examine the F-actin bundling activity of the CaMKII variants. The experimental results matched well with our expectations on the F-actin bundling capacities of CaMKII variants. Only the CaMKII variants with the native CaMKIIβ linker (i.e., CaMKIIα-long and CaMKIIβ) could bundle F-actin (Figures 4F and 4G). CaMKIIα-GGS could not bundle F-actin and could not rescue basal synaptic transmission and LTP in the DKO neurons (Figures 4D and 4E). Thus, it is the phase separation capacity, but not the F-actin bundling activity, responsible for the different roles played by CaMKII variants in basal synaptic transmission and LTP.

DISCUSSION

Extensive studies in the past have revealed that, both in CaMKIIα and CaMKIIβ, the kinase domain adopts a continuum of conformation with respect to the oligomeric hub domain.[17–19,44] The length of the unstructured linker between the kinase domain and the hub domain of CaMKII directly determines the "openness" of the holoenzyme. With respect to CaMKIIα, CaMKIIβ has a longer linker, and consequently, the enzyme adopts a more extended conformation and also is with higher conformational freedom.

Given the structural differences between CaMKIIα and CaMKIIβ, the goal of the present study was to determine the functional difference between these two isoforms and the structural basis underlying this difference. While CaMKIIα fully rescued the defects in basal synaptic transmission and LTP, CaMKIIβ failed to rescue the defects. Transplanting the short linker of CaMKIIα into CaMKIIβ restored synaptic functions, whereas transplanting the long linker of CaMKIIβ into CaMKIIα failed to restore synaptic functions. Critically, if a flexible "GGS" repeat of the same length as the CaMKIIβ linker is inserted into CaMKIIα, no rescue of synaptic function occurs. Thus, we conclude that the functional difference between CaMKIIα and CaMKIIβ resides solely in the length of the linker. How does the length of the linker have such a profound effect on the functional properties of these two isoforms?

It is well established that the binding of CaMKII to GluN2B is critical for the action of CaMKII.[7,32,33] Surprisingly, CaMKIIα and CaMKIIβ bind to the cytoplasmic tail of GluN2B with essentially the same affinity. However, when this interaction was examined with phase separation, there was a dramatic difference: the CaMKIIα/GluN2B complex, but not the CaMKIIβ/GluN2B complex, undergoes phase separation, forming condensed molecular assemblies. We further demonstrated that the length of the unstructured linker between the kinase domain and the hub domain determines the phase separation capacity of the CaMKII/GluN2B complexes. Our experimental observation is consistent with the core concept of biological condensates formation via phase separation. Phase separation of biomolecular complexes depends on multivalent interaction-mediated formation of large molecular networks.[45,46] Both CaMKIIα and CaMKIIβ exist predominantly as dodecamers formed by their hub domain, with a small population capable of forming tetradecamers.[17–19] GluN2B binds to the kinase domain of both CaMKIIα and CaMKIIβ. Thus, the length of the unstructured linker between the kinase domain and the hub domain determines the effective valences of CaMKII in binding to GluN2B. CaMKIIβ with a longer linker has a lower effective valency than CaMKIIα in binding to GluN2B and thus has a lower capacity in forming condensed assembly via phase separation (Figure S4). One might imagine that a CaMKII mutant with an infinitely long linker would have an effective valency of one in

Figure 4. CaMKIIα-GGS fails to rescue the defects in basal transmission and LTP induced by DKO

(A) Schematic diagram showing the design and domain organization of CaMKIIα-GGS.

(B and C) Confocal fluorescence images (B) and quantification data (C) showing that CaMKIIα with the GGS repeat insertion in the linker weakens its phase separation with GluN2B. The concentration of each protein in the assay was at 5 μM.

Statistical data in (C) are presented as mean ± SD, with results from 3 independent batches of experiments. ***$p < 0.001$; ****$p < 0.0001$ using two-tailed Student's t test.

(D) Scatterplots and bar graph of ratios normalized to control of the AMPAR EPSCs show amplitudes of AMPAR EPSC for single pairs (open circles) of control and transfected cells of DKO + CaMKIIα-GGS (n = 17 pairs). Filled circles indicate mean amplitude ± SEM (control = 93.4 ± 16; DKO + CaMKIIα-GGS = 39.7 ± 6.2, n = 21, $p < 0.0001$). Bar graph of ratios normalized to control (%) summarizing the mean ± SEM of AMPAR EPSCs for values represented in the scatterplot (52.6 ± 6). Raw amplitude data from dual-cell recordings were analyzed using Wilcoxon signed rank test (p values above). Scale bars: 20 ms, 50 mA.

(E) Plots show mean ± SEM AMPAR EPSC amplitude of control (black) and transfected (red) DKO + CaMKII-αGGS pyramidal neurons normalized to the mean AMPAR EPSC amplitude before LTP induction (control, n = 8; DKO + CaMKIIα-GGS, n = 8). Scale bars: 20 ms, 50 mA.

(F and G) Representative SDS-PAGE analysis (F) and quantification data (G) showing actin bundling by various CaMKII proteins using the high-speed centrifugation assay. The concentration of CaMKII was 2 μM, and the concentration of actin was 5 μM.

Statistical data in (C) and (G) are presented as mean ± SD, with results from 3 independent batches of experiments. ns, not significant; ***$p < 0.001$; ****$p < 0.0001$ using one-way ANOVA with Dunnett's multiple comparisons test.

See also Figure S4.

binding to GluN2B. In contrast, removing the linker between the kinase domain and the hub domain would increase the GluN2B binding valency of CaMKIIα to a theoretical maximum of twelve for the dodecameric enzyme. However, CaMKIIα with the linker domain removed adopts a much more compact conformation due to enhanced direct binding between the kinase domain and the hub domain,[18,44] causing the weakening of the interaction between the mutant CaMKIIα and GluN2B.

In addition to the effective interaction valences between CaMKII and GluN2B, the length of the unstructured linker may also affect the high-order oligomerization of CaMKII, a process that is mediated by the interactions between the kinase domains or between the kinase domain and the hub domain of two neighboring holoenzymes.[18,19] CaMKIIα with a shorter linker is more favorable of forming high-order enzyme clusters than CaMKIIβ.[19] Therefore, the short linker of CaMKIIα, when compared with the long linker in CaMKIIβ, could also promote the phase separation of the CaMKIIα/GluN2B complex by providing higher effective valences for the interaction between the CaMKII holoenzyme and for the interaction between CaMKII and GluN2B. We extrapolate, based on our *in vitro* biochemical and *in vivo* functional studies presented here, that activated CaMKIIα can form dense clusters with NMDARs in synapses via phase separation.[37,38] Such phase separation-mediated CaMKIIα/NMDAR nanodomain formation may support CaMKIIα-mediated synaptic transmission and LTP.

The present study has revealed the basis for why CaMKIIα, but not CaMKIIβ, rescues the deficits resulting from deleting CaMKII in hippocampal pyramidal cells. This raises the intriguing question as to what roles CaMKIIβ might play in neurons. Unlike excitatory neurons in the forebrain, it is well established that CaMKIIβ is the primary isoform expressed in cerebellar Purkinje cells[47] and that it has well-characterized roles in neuronal excitability and synaptic function.[48–50] However, the mechanism underlying these actions must be fundamentally different from the role of CaMKIIα in the hippocampus because Purkinje cells in young rodents lack NMDARs.[51,52]

Finally, in addition to answering a long-standing question in neuroscience regarding the roles of CaMKIIα and CaMKIIβ in synaptic physiology, our work also highlights how subtle sequence differences between CaMKIIα and CaMKIIβ can be harnessed by phase separation to express dramatically different physiological outcomes. In a broad perspective, our work suggests that divergent and unstructured linker sequences can play critical roles in determining the physiological functions among the different isoforms of proteins via phase separation.

Limitations of the study

The linkers between CaMKIIα and CaMKIIβ are linked to several distinct functional properties other than their different capacities in phase separating with NMDARs. For example, the two isoforms display different affinity and sensitivity for Ca^{2+}-CaM, different responses to Ca^{2+}-oscillation frequency,[18,53,54] differences in stimulatory and inhibitory autophosphorylation kinetics,[35] different affinities in binding to actin cytoskeleton,[25,26,36,42,43] etc. We have provided some evidence that differential actin cytoskeleton binding is unlikely a key determinant for the different roles of the two CaMKII isoforms in synaptic plasticity. However, one should not rule out that the remaining different properties of the two isoforms may also contribute to their distinct roles in synaptic plasticity.

STAR★METHODS

Detailed methods are provided in the online version of this paper and include the following:

- KEY RESOURCES TABLE
- RESOURCE AVAILABILITY
  - Lead contact
  - Materials availability
  - Data and code availability
- EXPERIMENTAL MODEL AND SUBJECT DETAILS
  - Mice
  - Bacterial strain
  - Cell line
- METHOD DETAILS
  - DNA constructs and peptide
  - Protein expression and purification
  - GST pull down assay
  - Isothermal titration calorimetry (ITC) assay
  - Protein labeling with chemical fluorophore
  - Phase separation assays
  - F-actin bundle sedimentation assay
  - Lentivirus production
  - P0 injection
  - Acute slice preparation
  - Slice culture preparation
  - Electrophysiological recording
- QUANTIFICATION AND STATISTICAL ANALYSIS

SUPPLEMENTAL INFORMATION

Supplemental information can be found online at https://doi.org/10.1016/j.celrep.2023.112146.

ACKNOWLEDGMENTS

This work was supported by a grant from National Science Foundation of China (82188101), the Minister of Science and Technology of China (2019YFA0508402), an HFSP Research Grant (RGP0020/2019), and grants from Research Grant Council of Hong Kong (AoE-M09-12, 16104518, and 16101419) to M.Z. and a grant from NIH (R01MH117139) to R.A.N.

AUTHOR CONTRIBUTIONS

Q.C., X.C., and S.Z. performed experiments; Q.C., X.C., R.A.N., and M.Z. analyzed data; Q.C., X.C., R.A.N., and M.Z. designed the research; Q.C., X.C., R.A.N., and M.Z. drafted the manuscript; M.Z. coordinated the project.

DECLARATION OF INTERESTS

The authors declare no competing interests.

Received: August 19, 2022
Revised: December 17, 2022
Accepted: February 6, 2023
Published: February 22, 2023

REFERENCES

1. Hell, J.W. (2014). CaMKII: claiming center stage in postsynaptic function and organization. Neuron *81*, 249–265. https://doi.org/10.1016/j.neuron.2013.12.024.
2. Bayer, K.U., and Schulman, H. (2019). CaM kinase: still inspiring at 40. Neuron *103*, 380–394. https://doi.org/10.1016/j.neuron.2019.05.033.
3. Lisman, J., Yasuda, R., and Raghavachari, S. (2012). Mechanisms of CaMKII action in long-term potentiation. Nat. Rev. Neurosci. *13*, 169–182. https://doi.org/10.1038/nrn3192.
4. Herring, B.E., and Nicoll, R.A. (2016). Long-term potentiation: from CaMKII to AMPA receptor trafficking. Annu. Rev. Physiol. *78*, 351–365. https://doi.org/10.1146/annurev-physiol-021014-071753.
5. Malenka, R.C., Kauer, J.A., Perkel, D.J., Mauk, M.D., Kelly, P.T., Nicoll, R.A., and Waxham, M.N. (1989). An essential role for postsynaptic calmodulin and protein kinase activity in long-term potentiation. Nature *340*, 554–557. https://doi.org/10.1038/340554a0.
6. Malinow, R., Schulman, H., and Tsien, R.W. (1989). Inhibition of postsynaptic PKC or CaMKII blocks induction but not expression of LTP. Science *245*, 862–866.
7. Incontro, S., Díaz-Alonso, J., Iafrati, J., Vieira, M., Asensio, C.S., Sohal, V.S., Roche, K.W., Bender, K.J., and Nicoll, R.A. (2018). The CaMKII/NMDA receptor complex controls hippocampal synaptic transmission by kinase-dependent and independent mechanisms. Nat. Commun. *9*, 2069. https://doi.org/10.1038/s41467-018-04439-7.
8. Kool, M.J., Proietti Onori, M., Borgesius, N.Z., van de Bree, J.E., Elgersma-Hooisma, M., Nio, E., Bezstarosti, K., Buitendijk, G.H.S., Aghadavoud Jolfaei, M., Demmers, J.A.A., et al. (2019). CAMK2-Dependent signaling in neurons is essential for survival. J. Neurosci. *39*, 5424–5439. https://doi.org/10.1523/JNEUROSCI.1341-18.2019.
9. Giese, K.P., Fedorov, N.B., Filipkowski, R.K., and Silva, A.J. (1998). Autophosphorylation at Thr286 of the alpha calcium-calmodulin kinase II in LTP and learning. Science *279*, 870–873.
10. Tao, W., Lee, J., Chen, X., Díaz-Alonso, J., Zhou, J., Pleasure, S., and Nicoll, R.A. (2021). Synaptic memory requires CaMKII. Elife *10*, e60360. https://doi.org/10.7554/eLife.60360.
11. Sanhueza, M., Fernandez-Villalobos, G., Stein, I.S., Kasumova, G., Zhang, P., Bayer, K.U., Otmakhov, N., Hell, J.W., and Lisman, J. (2011). Role of the CaMKII/NMDA receptor complex in the maintenance of synaptic strength. J. Neurosci. *31*, 9170–9178. https://doi.org/10.1523/JNEUROSCI.1250-11.2011.
12. Sanhueza, M., McIntyre, C.C., and Lisman, J.E. (2007). Reversal of synaptic memory by Ca2+/calmodulin-dependent protein kinase II inhibitor. J. Neurosci. *27*, 5190–5199. https://doi.org/10.1523/JNEUROSCI.5049-06.2007.
13. Bennett, M.K., Erondu, N.E., and Kennedy, M.B. (1983). Purification and characterization of a calmodulin-dependent protein kinase that is highly concentrated in brain. J. Biol. Chem. *258*, 12735–12744.
14. Brocke, L., Chiang, L.W., Wagner, P.D., and Schulman, H. (1999). Functional implications of the subunit composition of neuronal CaM kinase II. J. Biol. Chem. *274*, 22713–22722. https://doi.org/10.1074/jbc.274.32.22713.
15. Liu, N., and Cooper, N.G. (1994). Purification and characterization of the Ca2+/calmodulin-dependent protein kinase II from chicken forebrain. J. Mol. Neurosci. *5*, 193–206. https://doi.org/10.1007/BF02736733.
16. Lowenthal, M.S., Markey, S.P., and Dosemeci, A. (2015). Quantitative mass spectrometry measurements reveal stoichiometry of principal postsynaptic density proteins. J. Proteome Res. *14*, 2528–2538. https://doi.org/10.1021/acs.jproteome.5b00109.
17. Myers, J.B., Zaegel, V., Coultrap, S.J., Miller, A.P., Bayer, K.U., and Reichow, S.L. (2017). The CaMKII holoenzyme structure in activation-competent conformations. Nat. Commun. *8*, 15742. https://doi.org/10.1038/ncomms15742.
18. Sloutsky, R., Dziedzic, N., Dunn, M.J., Bates, R.M., Torres-Ocampo, A.P., Boopathy, S., Page, B., Weeks, J.G., Chao, L.H., and Stratton, M.M. (2020). Heterogeneity in human hippocampal CaMKII transcripts reveals allosteric hub-dependent regulation. Sci. Signal. *13*, eaaz0240. https://doi.org/10.1126/scisignal.aaz0240.
19. Buonarati, O.R., Miller, A.P., Coultrap, S.J., Bayer, K.U., and Reichow, S.L. (2021). Conserved and divergent features of neuronal CaMKII holoenzyme structure, function, and high-order assembly. Cell Rep. *37*, 110168. https://doi.org/10.1016/j.celrep.2021.110168.
20. Bhattacharyya, M., Stratton, M.M., Going, C.C., McSpadden, E.D., Huang, Y., Susa, A.C., Elleman, A., Cao, Y.M., Pappireddi, N., Burkhardt, P., et al. (2016). Molecular mechanism of activation-triggered subunit exchange in Ca(2+)/calmodulin-dependent protein kinase II. Elife *5*, e13405. https://doi.org/10.7554/eLife.13405.
21. Silva, A.J., Stevens, C.F., Tonegawa, S., and Wang, Y. (1992). Deficient hippocampal long-term potentiation in alpha-calcium-calmodulin kinase II mutant mice. Science *257*, 201–206. https://doi.org/10.1126/science.1378648.
22. Silva, A.J., Paylor, R., Wehner, J.M., and Tonegawa, S. (1992). Impaired spatial learning in alpha-calcium-calmodulin kinase II mutant mice. Science *257*, 206–211. https://doi.org/10.1126/science.1321493.
23. Pettit, D.L., Perlman, S., and Malinow, R. (1994). Potentiated transmission and prevention of further LTP by increased CaMKII activity in postsynaptic hippocampal slice neurons. Science *266*, 1881–1885.
24. Lledo, P.M., Hjelmstad, G.O., Mukherji, S., Soderling, T.R., Malenka, R.C., and Nicoll, R.A. (1995). Calcium/calmodulin-dependent kinase II and long-term potentiation enhance synaptic transmission by the same mechanism. Proc. Natl. Acad. Sci. USA *92*, 11175–11179.
25. Borgesius, N.Z., van Woerden, G.M., Buitendijk, G.H.S., Keijzer, N., Jaarsma, D., Hoogenraad, C.C., and Elgersma, Y. (2011). betaCaMKII plays a nonenzymatic role in hippocampal synaptic plasticity and learning by targeting alphaCaMKII to synapses. J. Neurosci. *31*, 10141–10148. https://doi.org/10.1523/JNEUROSCI.5105-10.2011.
26. Kim, K., Lakhanpal, G., Lu, H.E., Khan, M., Suzuki, A., Hayashi, M.K., Narayanan, R., Luyben, T.T., Matsuda, T., Nagai, T., et al. (2015). A temporary gating of actin remodeling during synaptic plasticity consists of the interplay between the kinase and structural functions of CaMKII. Neuron *87*, 813–826. https://doi.org/10.1016/j.neuron.2015.07.023.
27. Strack, S., and Colbran, R.J. (1998). Autophosphorylation-dependent targeting of calcium/calmodulin-dependent protein kinase II by the NR2B subunit of the N-methyl- D-aspartate receptor. J. Biol. Chem. *273*, 20689–20692.
28. Bayer, K.U., De Koninck, P., Leonard, A.S., Hell, J.W., and Schulman, H. (2001). Interaction with the NMDA receptor locks CaMKII in an active conformation. Nature *411*, 801–805.
29. Leonard, A.S., Lim, I.A., Hemsworth, D.E., Horne, M.C., and Hell, J.W. (1999). Calcium/calmodulin-dependent protein kinase II is associated with the N-methyl-D-aspartate receptor. Proc. Natl. Acad. Sci. USA *96*, 3239–3244.
30. Gardoni, F., Caputi, A., Cimino, M., Pastorino, L., Cattabeni, F., and Di Luca, M. (1998). Calcium/calmodulin-dependent protein kinase II is associated with NR2A/B subunits of NMDA receptor in postsynaptic densities. J. Neurochem. *71*, 1733–1741. https://doi.org/10.1046/j.1471-4159.1998.71041733.x.
31. Bayer, K.U., LeBel, E., McDonald, G.L., O'Leary, H., Schulman, H., and De Koninck, P. (2006). Transition from reversible to persistent binding of CaMKII to postsynaptic sites and NR2B. J. Neurosci. *26*, 1164–1174. https://doi.org/10.1523/JNEUROSCI.3116-05.
32. Halt, A.R., Dallapiazza, R.F., Zhou, Y., Stein, I.S., Qian, H., Juntti, S., Wojcik, S., Brose, N., Silva, A.J., and Hell, J.W. (2012). CaMKII binding to GluN2B is critical during memory consolidation. EMBO J. *31*, 1203–1216. https://doi.org/10.1038/emboj.2011.482.

33. Barria, A., and Malinow, R. (2005). NMDA receptor subunit composition controls synaptic plasticity by regulating binding to CaMKII. Neuron *48*, 289–301.

34. Cook, S.G., Bourke, A.M., O'Leary, H., Zaegel, V., Lasda, E., Mize-Berge, J., Quillinan, N., Tucker, C.L., Coultrap, S.J., Herson, P.S., and Bayer, K.U. (2018). Analysis of the CaMKIIalpha and beta splice-variant distribution among brain regions reveals isoform-specific differences in holoenzyme formation. Sci. Rep. *8*, 5448. https://doi.org/10.1038/s41598-018-23779-4.

35. Bhattacharyya, M., Lee, Y.K., Muratcioglu, S., Qiu, B., Nyayapati, P., Schulman, H., Groves, J.T., and Kuriyan, J. (2020). Flexible linkers in CaMKII control the balance between activating and inhibitory autophosphorylation. Elife *9*, e53670. https://doi.org/10.7554/eLife.53670.

36. O'Leary, H., Lasda, E., and Bayer, K.U. (2006). CaMKIIbeta association with the actin cytoskeleton is regulated by alternative splicing. Mol. Biol. Cell *17*, 4656–4665. https://doi.org/10.1091/mbc.e06-03-0252.

37. Cai, Q., Zeng, M., Wu, X., Wu, H., Zhan, Y., Tian, R., and Zhang, M. (2021). CaMKIIalpha-driven, phosphatase-checked postsynaptic plasticity via phase separation. Cell Res. *31*, 37–51. https://doi.org/10.1038/s41422-020-00439-9.

38. Hosokawa, T., Liu, P.W., Cai, Q., Ferreira, J.S., Levet, F., Butler, C., Sibarita, J.B., Choquet, D., Groc, L., Hosy, E., et al. (2021). CaMKII activation persistently segregates postsynaptic proteins via liquid phase separation. Nat. Neurosci. *24*, 777–785. https://doi.org/10.1038/s41593-021-00843-3.

39. Zeng, M., Shang, Y., Araki, Y., Guo, T., Huganir, R.L., and Zhang, M. (2016). Phase transition in postsynaptic densities underlies formation of synaptic complexes and synaptic plasticity. Cell *166*, 1163–1175.e12. https://doi.org/10.1016/j.cell.2016.07.008.

40. Zeng, M., Chen, X., Guan, D., Xu, J., Wu, H., Tong, P., and Zhang, M. (2018). Reconstituted postsynaptic density as a molecular platform for understanding synapse formation and plasticity. Cell *174*, 1172–1187.e16. https://doi.org/10.1016/j.cell.2018.06.047.

41. Zhu, J., Zhou, Q., Shang, Y., Li, H., Peng, M., Ke, X., Weng, Z., Zhang, R., Huang, X., Li, S.S.C., et al. (2017). Synaptic targeting and function of SAPAPs mediated by phosphorylation-dependent binding to PSD-95 MAGUKs. Cell Rep. *21*, 3781–3793. https://doi.org/10.1016/j.celrep.2017.11.107.

42. Shen, K., Teruel, M.N., Subramanian, K., and Meyer, T. (1998). CaMKII-beta functions as an F-actin targeting module that localizes CaMKIIalpha/beta heterooligomers to dendritic spines. Neuron *21*, 593–606. https://doi.org/10.1016/s0896-6273(00)80569-3.

43. Fink, C.C., Bayer, K.U., Myers, J.W., Ferrell, J.E., Jr., Schulman, H., and Meyer, T. (2003). Selective regulation of neurite extension and synapse formation by the beta but not the alpha isoform of CaMKII. Neuron *39*, 283–297. https://doi.org/10.1016/s0896-6273(03)00428-8.

44. Chao, L.H., Pellicena, P., Deindl, S., Barclay, L.A., Schulman, H., and Kuriyan, J. (2010). Intersubunit capture of regulatory segments is a component of cooperative CaMKII activation. Nat. Struct. Mol. Biol. *17*, 264–272. https://doi.org/10.1038/nsmb.1751.

45. Harmon, T.S., Holehouse, A.S., Rosen, M.K., and Pappu, R.V. (2017). Intrinsically disordered linkers determine the interplay between phase separation and gelation in multivalent proteins. Elife *6*, e30294. https://doi.org/10.7554/eLife.30294.

46. Chen, G., Wang, D., Wu, B., Yan, F., Xue, H., Wang, Q., Quan, S., and Chen, Y. (2020). Taf14 recognizes a common motif in transcriptional machineries and facilitates their clustering by phase separation. Nat. Commun. *11*, 4206. https://doi.org/10.1038/s41467-020-18021-7.

47. Burgin, K.E., Waxham, M.N., Rickling, S., Westgate, S.A., Mobley, W.C., and Kelly, P.T. (1990). In situ hybridization histochemistry of Ca2+/calmodulin-dependent protein kinase in developing rat brain. J. Neurosci. *10*, 1788–1798.

48. Pinto, T.M., Schilstra, M.J., Roque, A.C., and Steuber, V. (2020). Binding of filamentous actin to CaMKII as potential regulation mechanism of bidirectional synaptic plasticity by beta CaMKII in cerebellar Purkinje cells. Sci. Rep. *10*, 9019. https://doi.org/10.1038/s41598-020-65870-9.

49. Zybura, A.S., Baucum, A.J., Rush, A.M., Cummins, T.R., and Hudmon, A. (2020). CaMKII enhances voltage-gated sodium channel Nav1.6 activity and neuronal excitability. J. Biol. Chem. *295*, 11845–11865. https://doi.org/10.1074/jbc.RA120.014062.

50. Hirano, T., and Kawaguchi, S.Y. (2014). Regulation and functional roles of rebound potentiation at cerebellar stellate cell-Purkinje cell synapses. Front. Cell. Neurosci. *8*, 42. https://doi.org/10.3389/fncel.2014.00042.

51. Hartmann, J., and Konnerth, A. (2005). Determinants of postsynaptic Ca2+ signaling in Purkinje neurons. Cell Calcium *37*, 459–466. https://doi.org/10.1016/j.ceca.2005.01.014.

52. Perkel, D.J., Hestrin, S., Sah, P., and Nicoll, R.A. (1990). Excitatory synaptic currents in Purkinje cells. Proc. Biol. Sci. *241*, 116–121. https://doi.org/10.1098/rspb.1990.0074.

53. De Koninck, P., and Schulman, H. (1998). Sensitivity of CaM kinase II to the frequency of Ca2+ oscillations. Science *279*, 227–230. https://doi.org/10.1126/science.279.5348.227.

54. Bayer, K.U., De Koninck, P., and Schulman, H. (2002). Alternative splicing modulates the frequency-dependent response of CaMKII to Ca(2+) oscillations. EMBO J. *21*, 3590–3597. https://doi.org/10.1093/emboj/cdf360.

55. Chao, L.H., Stratton, M.M., Lee, I.H., Rosenberg, O.S., Levitz, J., Mandell, D.J., Kortemme, T., Groves, J.T., Schulman, H., and Kuriyan, J. (2011). A mechanism for tunable autoinhibition in the structure of a human Ca2+/calmodulin- dependent kinase II holoenzyme. Cell *146*, 732–745. https://doi.org/10.1016/j.cell.2011.07.038.

56. Stoppini, L., Buchs, P.A., and Muller, D. (1991). A simple method for organotypic cultures of nervous tissue. J. Neurosci. Methods *37*, 173–182.

STAR★METHODS

KEY RESOURCES TABLE

REAGENT or RESOURCE	SOURCE	IDENTIFIER
Bacterial and virus strains		
Escherichia coli: BL21-CodonPlus(DE3)-RIL	Agilent	Cat# 230245
Escherichia coli: DH10Bac	Thermo Fisher	Cat# 10361012
Chemicals, peptides, and recombinant proteins		
Chemical: Alexa Fluor 647 NHS Ester	Thermo Fisher Scientific	Cat# A20106
Chemical: iFluor 405 NHS Ester	AAT Bioquest	Cat# 1021
Chemical: iFluor 488 NHS Ester	AAT Bioquest	Cat# 1023
Chemical: Cy3 NHS Ester	AAT Bioquest	Cat# 271
Peptide: GluN2Bpep (KAQKKNRNKLRRQHSYDTFVDL)	ChinaPeptides	N/A
Recombinant protein: CaMKIIα	Cai et al., 2021[37]	N/A
Recombinant protein: CaMKIIβ	This paper	N/A
Recombinant protein: CaMKIIα-long	This paper	N/A
Recombinant protein: CaMKIIβ-short	This paper	N/A
Recombinant protein: CaMKIIα-GK	This paper	N/A
Recombinant protein: CaMKIIα-GGS	This paper	N/A
Recombinant protein: GluN2B (1170–1482)	Cai et al.[37]	N/A
Recombinant protein: GluN2B-DLS	This paper	N/A
Recombinant protein: CaM	Cai et al.[37]	N/A
Recombinant protein: PSD-95	Zeng et al.[40]	N/A
Recombinant protein: SAPAP	This paper	N/A
Recombinant protein: Shank3	Zeng et al.[40]	N/A
Recombinant protein: Homer3	Zeng et al.[40]	N/A
Critical commercial assays		
Helios Gene Gun Kit	Bio-Rad	Cat# 1652411
Helios Cartridge Kit	Bio-Rad	Cat# 1652440
Experimental models: Cell lines		
Sf9 cells	Thermo Fisher	Cat# 12659017
High Five cells	Thermo Fisher	Cat# B85502
Experimental models: Organisms/strains		
B6J.129(Cg)-Gt(ROSA)$^{26Sortm1.1(CAG-cas9*,-EGFP)Fezh}$/J	The Jackson Laboratory	Strain# 026179
Recombinant DNA		
pSUMO-CaMKIIα	Cai et al.[37]	N/A
pFastbac-SUMO*-CaMKIIβ	This paper	N/A
pSUMO-CaMKIIα-long	This paper	N/A
pSUMO-CaMKIIβ-short	This paper	N/A
pSUMO-CaMKIIα-GK	This paper	N/A
pSUMO-CaMKIIα-GGS	This paper	N/A
pMG3C-GluN2B (1170–1482)	Cai et al.[37]	N/A
pMG3C-GluN2B-DLS	This paper	N/A
32M3C-CaM	Cai et al.[37]	N/A
32M3C-PSD-95	Zeng et al.[40]	N/A
32M3C-SAPAP	Zeng et al.[40]	N/A
pMG3C-Shank3	Zeng et al.[40]	N/A
M3C-Homer3	Zeng et al., 2018[40]	N/A

(*Continued on next page*)

Continued		
REAGENT or RESOURCE	SOURCE	IDENTIFIER
pFUGW-CaMKII 2gRNA-IRES-mCherry	Incontro et al.[7]	N/A
pFUGW-CaMKII 2gRNA-Ubqt-CaMKIIα-IRES-mCherry	This paper	N/A
pFUGW-CaMKII 2gRNA-Ubqt-CaMKIIβ-IRES-mCherry	This paper	N/A
pFUGW-CaMKII 2gRNA-Ubqt-CaMKIIα-long-IRES-mCherry	This paper	N/A
pFUGW-CaMKII 2gRNA-Ubqt-CaMKIIβ-short-IRES-mCherry	This paper	N/A
pFUGW-CaMKII 2gRNA-Ubqt-CaMKIIα-GGS-IRES-mCherry	This paper	N/A
Software and algorithms		
ImageJ	NIH	https://imagej.nih.gov/ij/
Prism	GraphPad	https://www.graphpad.com/scientific-software/prism/
Origin 7.0	OriginLab	https://www.originlab.com/
Other		
HiLoad 26/600 Superdex 75 pg	Cytiva	Cat# 28989334
HiLoad 26/600 Superdex 200 pg	Cytiva	Cat# 28989336
HiTrap Desalting	Cytiva	Cat# 17140801
Nanodrop One C	Thermo Fisher	Cat# 840–317500

RESOURCE AVAILABILITY

Lead contact

Further information and requests for resources and reagents should be directed to and will be fulfilled by the lead contact, Mingjie Zhang (zhangmj@sustech.edu.cn).

Materials availability

Plasmids generated in this study are available upon request. Requests for plasmids should be directed to and will be fulfilled by the lead contact.

Data and code availability

- All data reported in this paper will be shared by the lead contact upon request.
- This paper does not report original code.
- Any additional information required to reanalyze the data reported in this paper is available from the lead contact upon request.

EXPERIMENTAL MODEL AND SUBJECT DETAILS

Mice

Both male and female B6J.129(Cg)-Gt(ROSA)$^{26Sortm1.1(CAG-cas9*,-EGFP)Fezh}$/J mice (The Jackson Laboratory) with the age of 18–45 days were used in this study. All mice were maintained under a 12:12 h L/D schedule according to the University of California, San Francisco IACUC guidelines. All protocols were approved by the IACUC at University of California, San Francisco, in full compliance with NIH guidelines for humane treatment of animals.

Bacterial strain

Escherichia coli BL21-CodonPlus(DE3)-RIL cells (Agilent) were used in this study for the production of recombinant proteins. DH10Bac cells (Thermo Fisher) were used for recombinant bacmid production. Cells were cultured in LB medium supplemented with necessary antibiotics.

Cell line

Sf9 cells (Thermo Fisher) were used in this study to produce the recombinant baculovirus. The sf9 cells were cultured in Sf-900 III SFM medium (Thermo Fisher). High Five cells (Thermo Fisher) were used in this study for the production of recombinant proteins. The High Five cells were cultured in Express Five SFM medium (Thermo Fisher).

METHOD DETAILS

DNA constructs and peptide

The cDNA sequences of rat CaMKIIα (Uniprot: P11275) and mouse CaMKIIβ (Uniprot: P28652) were PCR-amplified from rat and mouse brain cDNA library. All variants of full length CaMKII encoding constructs were generated by the standard PCR method. Each resulting CaMKII construct was inserted into the pEGFP-C3 vector with an N-terminal EGFP tag for HEK 293T cell expression or a pET vector with an N-terminal His_6-SUMO tag for *Escherichia coli* expression except for CaMKIIβ. DNA fragment encoding the full length CaMKIIβ was inserted into a modified pFastbac HT A vector with the TEV protease cutting site replaced by an HRV-3C protease cutting site followed by an N-terminal SUMO tag for baculovirus expression. Constructs encoding various fragments of CaMKII were generated by the standard PCR method and inserted into a pET vector with N-terminal His_6 tag and an HRV-3C protease cutting site.

The chimeric constructs of CaMKII with the kinase and AIS domains (a.a. 1–314 for CaMKIIα and a.a. 1–315 for CaMKIIβ) replaced by the PSD-95 GK domain (a.a. 531–713 of human PSD-95) by the overlap PCR method and inserted into a pET vector with an N-terminal His_6-SUMO tag for *Escherichia coli* expression. For the GluN2B-DLS construct, the cDNA sequence of DLS peptide[41] was inserted between a.a. 1310 and 1311 of GluN2B by the standard PCR method.

For the constructs used for electrophysiological experiments, the DNA fragments of all variants of the full length CaMKII were inserted into the pFUGW-CaMKII 2gRNA[7] and controlled by ubiquitin promoter, which followed by IRES-mCherry sequence (Figure 1B).

All other constructs are the same as previously reported.[37,40] All constructs were confirmed by DNA sequencing.

The GluN2Bpep peptide (sequence: KAQKKNRNKLRRQHSYDTFVDL) was commercially synthesized by ChinaPeptides (Shanghai, China) with purity >99%.

Protein expression and purification

All variants of CaMKII holoenzyme, except for CaMKIIβ, were expressed and purified according to the previous reported protocols.[37,55] Briefly, variants of CaMKII with N-terminal His_6-SUMO tag were co-expressed with λ phosphatase in *Escherichia coli* BL21-CodonPlus(DE3)-RIL cells (Agilent Technologies) in LB medium at 16°C for 24 h. The recombinant CaMKII proteins were extracted by high pressure homogenizer and purified by Ni^{2+}-NTA Sepharose 6 Fast Flow resin (Cytiva) and Superdex 200 26/600 (Cytiva) gel filtration chromatography. After the His_6-SUMO tag was removed by Ulp1 protease, proteins were further purified by Mono Q anion exchange chromatography and Superose 6 10/300 gel filtration chromatography. The final column buffer and also as the storage buffer was 50 mM Tris pH 8.0, 200 mM NaCl, 10% glycerol, 5 mM DTT. CaMKIIβ holoenzyme was expressed by Bac-to-Bac baculovirus expression system. The recombinant virus was obtained by transposition, transfection, and serial steps of amplification using sf9 cells (Thermo Fisher) according to the manufacturer's instructions. High Five cells (Thermo Fisher) with the density of 2.0×10^6 cells per mL were infected by baculovirus and incubated at 27°C for 60 h. The purification of CaMKIIβ was similar as the other CaMKII proteins.

All other proteins were expressed in *Escherichia coli* BL21-CodonPlus(DE3)-RIL cells (Agilent Technologies) in LB medium at 16°C overnight, except that GluN2B was expressed at 37°C for 2 h. Recombinant proteins were firstly purified using Ni^{2+}-NTA Sepharose 6 Fast Flow affinity chromatography (Cytiva) for His_6-tagged proteins or Glutathione Sepharose 4 Fast Flow affinity chromatography (Cytiva) for GST-tagged proteins and followed by a step of gel filtration chromatography using Superdex 200 26/600 or Superdex 75 26/600 column (Cytiva). The tag of each protein was cleaved by HRV-3C protease at 4°C overnight and removed by another step of gel filtration chromatography.

GST pull down assay

GST pull down assay was carried out as previously described.[37] Briefly, HEK293T cells were transiently transfected with various GFP-CaMKII encoding plasmids using Lipofectamine and Plus reagents (Thermo Fisher), then harvested at 20 h post transfection and lysed using the lysis buffer containing 50 mM Tris pH 7.5, 150 mM NaCl, 1% Triton X-100 and a cocktail of protease inhibitors (Merck). The mixture of lysate and GST-fused protein was incubated at 4°C for 30 min. After centrifugation at 16,873 g for 5 min, the supernatant was mixed with 40 μL of fresh Glutathione Sepharose resin and incubated for another 30 min. After extensive washing, the captured proteins were eluted by SDS-PAGE loading buffer by boiling, resolved by SDS-PAGE, and immunoblotted with specific antibodies. Protein signals were visualized by an HRP-conjugated secondary antibody (Thermo Fisher) and Luminata Forte western HRP substrate (Merck)

Isothermal titration calorimetry (ITC) assay

ITC experiments were carried out using a VP-ITC calorimeter (Malvern) at 25°C. All proteins used in the ITC experiments were in the buffer containing 50 mM Tris pH 8.0, 100 mM NaCl, 2 mM DTT and 2 mM $CaCl_2$. Each titration point was performed by injecting a 10 μL aliquot of one protein in the syringe into its binding protein in the cell at a time interval of 120 s to ensure that the titration peak returned to the baseline. Titration data were fitted with the one-site binding model using Origin 7.0 to derive the K_d values.

Protein labeling with chemical fluorophore

The chemical fluorophores, including iFluor 488/Cy3/Cy5 NHS esters (AAT Bioquest), were dissolved in DMSO at the concentration of 10 mg/mL. A HiTrap desalting column (Cytiva) was used to replace 50 mM Tris with 100 mM $NaHCO_3$ pH 8.3 while the rest of the buffer components were kept the same for each purified protein. A fluorophore was mixed with a specific protein at a 1:1 M ratio and incubated at room temperature for 1 h. After quenching by 0.2 M Tris pH 8.0, the labeled protein was exchanged into the storage buffer using a HiTrap Desalting column (Cytiva). Fluorescence labeling efficiency was detected using Nanodrop OneC (Thermo Fisher).

Phase separation assays

In vitro phase separation assays were carried out according to our previous reported protocols.[39,40] Briefly, all purified proteins were pre-cleared by high-speed centrifugation (16,873 g for 10 min) at 4°C in their storage buffer prior to phase separation assays. Proteins were directly mixed to reach specified protein concentrations. For phase separation assays, the NaCl concentration of the final buffer was carefully adjusted to reach specified concentration. Fresh DTT was added to the final concentration of 2 mM to avoid potential protein aggregation and precipitation.

For sedimentation-based assays, the total volume of each mixture is 30 μL. After incubation at room temperature for 10 min, the mixture was centrifuged at 16,873 g at 22°C for 5 min. The supernatant was collected, and the pellet was resuspended with 30 μL buffer. Samples from supernatant fraction and pellet fraction were analyzed by SDS-PAGE with Coomassie blue R250 staining. Three repeats were performed for each group. The intensity of each band on SDS-PAGE was quantified by ImageJ and data were presented as mean ± SD.

For confocal microscope-based assay, the total volume of each mixture is 20 μL. Each mixture was injected into a home-made chamber composed of a coverslip and a glass slide assembled with one layer of double-sided tape. The confocal fluorescent images were captured at room temperature using a Zeiss LSM 880 confocal microscope with a 63 × 1.4 N.A. oil objective. The integrated fluorescence intensities in droplets were quantified by ImageJ and data were presented as mean ± SD.

F-actin bundle sedimentation assay

Rabbit skeletal muscle actin (Cytoskeleton) was dissolved in the buffer containing 5 mM Tris, pH 8.0, 0.2 mM $CaCl_2$, 0.2 mM ATP and 0.5 mM DTT with the concentration of 20 μM and centrifuged at 16,873 g for 10 min at 4°C. Actin was polymerized at room temperature for 1 h in the polymerizing buffer containing 50 mM KCl, 2 mM $MgCl_2$, 1 mM ATP and 0.5 mM DTT. Actin bundles was prepared by mixing 5 μM F-actin with 2 μM CaMKII variants at room temperature for 1 h with the total volume of 25 μL. The mixture was centrifuged at 10,000 g at 22°C for 20 min. The supernatant was collected, and the pellet was resuspended with 25 μL buffer. Samples from supernatant fraction and pellet fraction were analyzed by SDS-PAGE with Coomassie blue R250 staining. Three repeats were performed for each group. The intensity of each band on SDS-PAGE was quantified by ImageJ and data were presented as mean ± SD.

Lentivirus production

Three T-75 flasks of rapidly dividing HEK293T cells (ATCC) were transfected with 27 mg FUGW-CaMKII 2gRNA-CaMKII variant-mCherry, plus helper plasmids pVSV-G (18 mg) and psPAX2 (27 mg) using FuGENE HD (Promega). DNA was incubated with 210 mL FuGENE HD in 4.5 mL Opti-MEM (Life Technologies) before transfection, according to the manufacturer's directions. Forty hours later, supernatant was collected, filtered, and concentrated using the PEG-it Virus Precipitation Solution (System Biosciences) according to the manufacturer's directions. The resulting pellet was resuspended in 150 mL Opti-MEM, flash-frozen with dry ice, and stored at −80°C.

P0 injection

Rosa26-Cas9 knock-in mice (B6J.129(Cg)-Gt(ROSA)$^{26Sortm1.1(CAG-cas9*,-EGFP)Fezh}$/J) were used. The mice of both sexes were purchased from the Jackson Laboratory (Stock No. 026179). These mice constitutively express Cas9 and GFP. Concentrated lentiviruses were injected bilaterally into the medial hippocampi of hypothermia anesthetized P0-P1 pups, by free hand. 2 μL per hemisphere was slowly delivered. All experiments were performed in accordance with established protocols approved by the University of California San Francisco Institutional Animal Care and Use Committee.

Acute slice preparation

Acute hippocampal slices were prepared from P18-P28 mice. Adult mice were anesthetized with isoflurane and decapitated. While submerged in cutting solution, brains were removed and sliced into 300 μm near-horizontal sections using Microslicer DTK-Zero1 (Ted Pella). Slices were then transferred to a holding chamber containing ACSF (125 mM NaCl, 2.5 mM KCl, 1.25 mM NaH_2PO_4, 25 mM $NaHCO_3$, 11 mM glucose, 1 mM $MgSO_4$, 2 mM $CaCl_2$ saturated with 95% O_2/5% CO_2) and incubated for 20 min at 37ºC and then kept at room temperature until use.

Slice culture preparation

Hippocampal organotypic slice cultures were prepared from 7–9 day old mice as previously described.[56] Transfections were carried out 48 h after culturing using a Helios Gene Gun (Bio-Rad) with 1-μm DNA-coated gold particles. Slices were maintained at 34ºC with media changes every two days.

Electrophysiological recording

All electrophysiological recordings were carried out on an upright Olympus BX51WI microscope and collected using a Multiclamp 700B amplifier (Molecular Devices). During recording, slices were maintained in ACSF containing 125 mM NaCl, 2.5 mM KCl, 1.25 mM NaH_2PO_4, 25 mM $NaHCO_3$, 11 mM glucose saturated with 95% O_2/5% CO_2) containing 1 mM $MgSO_4$, 2 mM $CaCl_2$ during acute recordings and 4 mM $MgSO_4$, 4 mM $CaCl_2$ during slice culture recordings. Transfected cells were identified visually using fluorescence and recorded simultaneously with a neighboring control cell. All recordings were carried out at 20–25 ºC using glass patch electrodes filled with an intracellular solution containing 135 mM $CsMeSO_3$, 10 mM HEPES, 8 mM NaCl, 0.3 mM EGTA, 4 mM Mg-ATP, 0.3 mM Na-GTP, 5 mM QX-314, and 0.1 mM spermine). Synaptic currents were elicited by stimulation of the Schaffer collaterals with a bipolar electrode (Micro Probes). AMPAR-mediated responses were collected in the presence of 100 μM picrotoxin to block inhibition. 4 μM 2-Chloroadenosine was used to suppress epileptic activity in slice culture. Bipolar stimulating electrode was placed in stratum radiatum or stratum moleculare of recording cells. AMPAR EPSCs were evoked while voltage clamping cells at −70 mV, and the amplitude was determined by measuring the peak of this response. Series resistances typically ranged from 10 to 20 MΩ; a cell pair was discarded if the series resistance of either increased to >30 MΩ.

LTP was induced via a pairing protocol of 2 Hz stimulation for 90 s at a holding potential of 0 mV, after recording a 3–5 min baseline, but not more than 6 min after breaking into the cell. All LTP experiments were carried out in acute slices. Simultaneous dual whole-cell recordings were made in a transfected CA1 pyramidal cell and a neighboring wild-type cell. In some cases, one of the paired cells was lost during the experiment, then the recordings were considered until that point. In cases where one cell was lost the remaining cell was considered for the averages.

QUANTIFICATION AND STATISTICAL ANALYSIS

Statistical parameters including the definitions and exact values of n (e.g. number of experiments), distributions and deviations are reported in the Figures and corresponding Figure Legends. Statistical analysis was performed in GraphPad Prism.